Far sidelobe effects from panel gaps of the Atacama Cosmology Telescope

Fluxa Rojas, Pedro Antonio, Dünner, Rolando, Maurin, Loïc, Choi, Steve, Devlin, Mark, et al.

Pedro Antonio Fluxa Rojas, Rolando Dünner, Loïc Maurin, Steve K. Choi, Mark J. Devlin, Patricio A. Gallardo, Shuay-Pwu P. Ho, Brian J. Koopman, Thibaut Louis, Jeffrey J. McMahon, Federico Nati, Michael D. Niemack, Laura Newburgh, Lyman A. Page, Maria Salatino, Alessandro Schillaci, Benjamin L. Schmitt, Sara M. Simon, Suzanne T. Staggs, Edward J. Wollack, "Far sidelobe effects from panel gaps of the Atacama Cosmology Telescope," Proc. SPIE 9914, Millimeter, Submillimeter, and Far-Infrared Detectors and Instrumentation for Astronomy VIII, 99142Q (19 July 2016); doi: 10.1117/12.2231421

SPIE.

Event: SPIE Astronomical Telescopes + Instrumentation, 2016, Edinburgh, United Kingdom

Far sidelobe effects from panel gaps of the Atacama Cosmology Telescope

Pedro Fluxá R.[a], Rolando Dünner[a], Loïc Maurin[a], Steve K. Choi[b], Mark J. Devlin[c], Patricio A. Gallardo[d], Shuay-Pwu P. Ho[b], Brian J. Koopman[d], Thibaut Louis[e], Jeffrey J. McMahon[f], Federico Nati [c], Michael D. Niemack [d], Laura Newburgh[g], Lyman A. Page[b], Maria Salatino[b], Alessandro Schillaci [a], Benjamin L. Schmitt [c], Sara M. Simon [b], Suzanne T. Staggs [b], and Edward J. Wollack[h]

[a]Instituto de Astrofísica and Centro de Astro-Ingeniería, Facultad de Física, Pontificia Universidad Católica de Chile, Av. Vicuña Mackenna 4860, 7820436 Macul, Santiago, Chile
[b]Department of Astrophysical Sciences, Peyton Hall, Princeton University, Princeton, NJ USA 08544
[c]Department of Physics and Astronomy, University of Pennsylvania, 209 South 33rd Street, Philadelphia, PA, USA 19104
[d]Department of Physics, Cornell University, Ithaca, NY, USA 14853
[e]Sub-department of Astrophysics, University of Oxford, Keble Road, Oxford, OX1 3RH, UK
[f]Department of Physics, University of Michigan Ann Arbor, MI 48109, USA
[g]Dunlap Institute for Astronomy & Astrophysics, University of Toronto, Toronto, ON M5S 3H4, Canada
[h]NASA/Goddard Space Flight Center, Greenbelt, MD 20771, USA

ABSTRACT

The Atacama Cosmology Telescope is a 6 meter diameter CMB telescope located at 5200 meters in the Chilean desert. ACT has made arc-minute scale maps of the sky at 90 and 150 GHz which have led to precise measurements of the fine angular power spectrum of the CMB fluctuations in temperature and polarization. One of the goals of ACT is to search for the B-mode polarization signal from primordial gravity waves, and thus extending ACT's data analysis to larger angular scales. This goal introduces new challenges in the control of systematic effects, including better understanding of far sidelobe effects that might enter the power spectrum at degree angular scales. Here we study the effects of the gaps between panels of the ACT primary and secondary reflectors in the worst case scenario in which the gaps remain open. We produced numerical simulations of the optics using GRASP up to 8 degrees away from the main beam and simulated timestreams for observations with this beam using real pointing information from ACT data. Maps from these simulated timestreams showed leakage from the sidelobes, indicating that this effect must be taken into consideration at large angular scales.

Keywords: Cosmology, Cosmic Microwave Background, Polarization, B-modes, Optical Simulations, Far-sidelobes, Diffraction, Electromagnetic simulations

1. INTRODUCTION

The Atacama Cosmology Telescope (ACT) is a 6 m off-axis, aplanatic, Gregorian telescope designed to have a large field of view and fast compact optics (f/2.5) for rapid scanning, which allows for the production of arc-minute resolution maps of the Cosmic Microwave Background (CMB)[1,2] at millimeter wavelengths. Its optical design was optimized to achieve high angular resolution maps with consistent beam shape an minimal sidelobe pickup,[3]

Further author information:
Pedro Fluxá: E-mail: pafluxa@astro.puc.cl
Rolando Dünner: E-mail : rdunner@astro.puc.cl

Millimeter, Submillimeter, and Far-Infrared Detectors and Instrumentation for Astronomy VIII, edited by Wayne S. Holland, Jonas Zmuidzinas, Proc. of SPIE Vol. 9914, 99142Q
 · doi: 10.1117/12.2231421

with two layers of ground shielding protecting it from spurious signals from the surroundings. It is located at 5200 m in Northern Chile and has been operating since 2007, when the first three-band camera (MBAC) was installed. In 2013, MBAC was replaced by a new polarization sensitive receiver (ACTpol)[4] containing two 150 GHz optic tubes and one 90/150 GHz multi-chroic system, each with detector arrays containing more that a thousand TES bolometers operating at 100 mK.

Starting in 2016, the receiver will be upgraded in stages to the new generation of Advanced ACTpol camera[5] with an increased number of detectors, higher sensitivities, and multi-chroic frequencies ranging from 30 to 220 GHz. This new experiment aims to measure the CMB polarization with unprecedented precision, measuring, among other things, the B-mode signal generated by both the gravitational lensing effect from the foreground large scale structure and primordial gravitational waves that might have been generated during the epoch of Inflation. Measurements of primordial B-modes requires sensitivity on scales of several degrees. So far ACT measurements have been restricted to relatively small angular scales (multipoles > 225), to extract signals at degree angular scales.

This work studies the effects of the gaps between the panels that compose the primary and secondary reflectors of the telescope. These gaps can asymmetrically diffract light over broad incidence angles.[6] The panel gaps in ACT are covered with aluminum tape, but we perform these simulations in the limiting case of no tape, to provide an upper limit to the effect. We do this based on numerical simulations that extend as far as 8 degrees away from the center of the beam, producing a non-polarized, asymmetric version of the beam. To understand its effects on the maps, we simulate Time Ordered Data (TOD) for observations of a simulated CMB sky realization with this beam using real pointing information from ACT data, and then reproject the TOD onto a map. In this way, we correctly reproduce the expected averaging of the beam due to the different pointing angles and detector polarization angles that reach every pixel of the map. The resulting maps are analyzed to quantify the amount of power and temperature to polarization leakage picked up by the sidelobes.

In Section 2, we describe the ACT optics and the simulations done to understand the diffracted beam. In Section 3, we describe the method used to produce simulated maps using real pointing data. In Section 4, we provide conclusions and considerations for the ACT data analysis.

2. ACT OPTICS AND SIMULATION

The ACT optics comprise a 6 m primary reflector, illuminating a 2 m secondary reflector, which in turn illuminates the receiver. The receiver contains three optics tubes, each one containing refractive optics to re-image light onto a separate detector array. The primary aperture is defined by a cold Lyot stop, limiting the amount of spillover around the reflector. The optics tubes form a triangle, with the two lower ones placed symmetrically at either side and the upper one centered. In ACTpol, the upper tube is the 90/150 GHz multichroic array (AR3), which is the one considered for this study.

Given the size of the ACT reflectors, it was impractical to make them from a single block of aluminum, so both the primary and secondary reflectors are formed by aluminum panels, 71 for the former and 11 for the latter, as shown in Figure 1. Also, a reflector made of panels allows a fine adjustment of its shape to compensate mechanical deformations that downgrade system performance. There is a small separation gap between the panels of ≈ 2 mm for the primary and ≈ 1 mm for the secondary. The electrical discontinuity of the gaps can produce diffraction effects, which might also be polarized. To reduce this effect the gaps were covered with aluminum tape (0.1 mm thick metallization), whose electrical properties are not fully characterized.

2.1 GRASP simulations

We used the commercial Electromagnetic (EM) Simulation software GRASP (v10.3)* to simulate the ACT optics. The simulation included both reflective and refractive optics up to the focal plane, excluding the feedhorn-detector system, for the 90 GHz optics, as shown in Figure 1. To provide an upper limit to this effect, we simulated the case in which no tape is used to cover the gaps. Primary and secondary panels were defined individually, leaving the corresponding gap separation between them.

*www.ticra.com

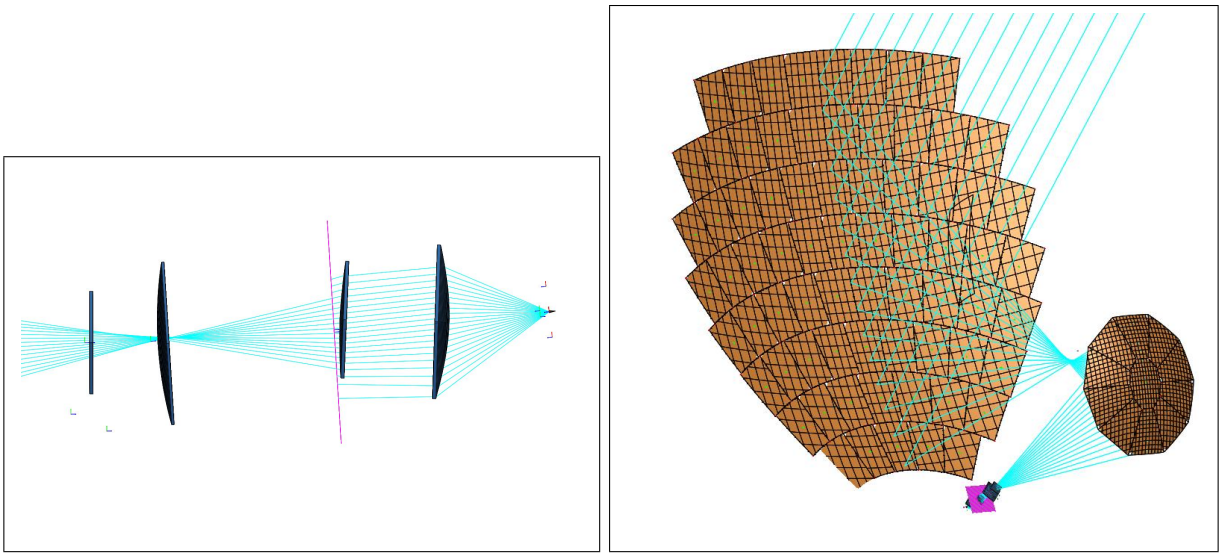

Figure 1. Left: Ray-trace of refractive optics for the 90GHz detectors in the AR3 optics tube of ACTpol. The leftmost lens is the camera window. Right: ray-trace of ACT, showing the 71 panels of the primary reflector and the 11 of the secodary reflector.

Given that the size of the reflectors is much larger than the wavelength (of order of 1000 λ for 90 Ghz), it is computationally impractical to run a full electromagnetic simulation of this problem. Geometrical Optics (ray tracing) works well for high frequency problems, but it does only a rough approximation of discontinuities in the surface currents of a reflector like the panel gaps. Physical Optics (PO) improves this by recalculating the currents on each surface before propagating the fields to the next one, taking into consideration the current discontinuity, but neglecting diffraction effects on the edges. This is improved even further by using Physical Theory of Diffraction (PTD), which incorporates edge currents on the gaps and its diffraction effects, but its execution was exceedingly long when the gaps from both reflectors were included. For this reason we decided to baseline using PO, even though it will only provide a lower limit to the amount of sidelobe power from the gaps, and does not reproduce correctly the beam polarization, forcing us to work with an unpolarized beam.

The panels gaps are expected to produce large sidelobes at wide angles from the main beam, but with significantly less amplitude than the main beam peak. This implies that the calculation must converge over a large dynamic range, which is computationally expensive. To prevent this, we forced GRASP to check for convergence of the the far field 0.25 degrees away from the center of the beam. The far sidelobe beam was computed on a HEALPIX[7] polar cap of 16 degrees in diameter.

Given that we are interested in phenomena occurring mostly at degree angular scales, we were not forced to fully resolve the beam center. The resolution of the beam map was set to 1.7 arc-minutes per pixel (HEALPIX cap with NSIDE=2048), which is smaller than the 2' Full Width Half Maximum (FWHM) expected for 90 GHz. This resolution is small enough to reduce pixelization errors in subsequent analysis, but coarse enough to speed up the computation.

GRASP simulations were performed on *hades*, a node dedicated for EM simulations located at the computing center of the Centro de Astrongenieria at PUC. *Hades* has 64 AMD 6380 Opteron processors, 128 GB RAM and a 20 TB RAID5 array. For all simulations, convergence level was always better than 60 dB with respect to the grid peak. The simulation time for the complete beam with gaps on both reflectors was about 5 hours using PO for a monochromatic at 90 GHz.

Figure 2 shows the resulting beams from simulating gaps in only one of the reflectors or in both, respectively. We observe that the sidelobes from gaps in the primary are very extended, reaching more than 30 degrees away from the center (not shown in the figure), with vertical symmetry as expected from the telescope's symmetry.

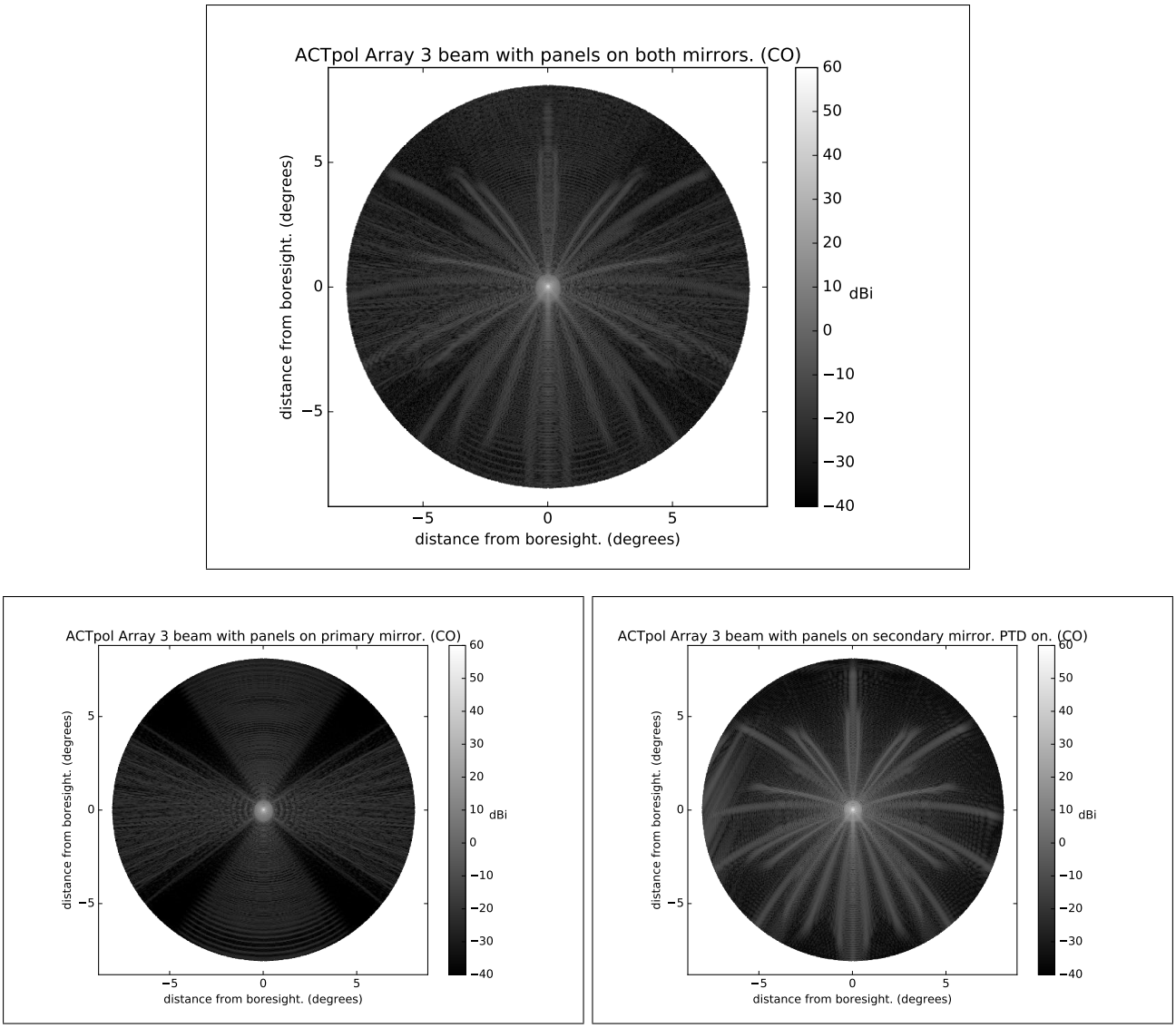

Figure 2. Up: Full simulated co-polar beam for ACTpol's 90 GHz AR3 central detector, including uniform 2 mm gaps in both primary and secondary reflectors. The simulation was done with GRASP v10.3 and used Physical Optics to estimate the diffraction from the panel gaps. Lower left: Co-polar beam when only gaps on the primary reflector are included. Lower right: Co-polar beam when only gaps on the secondary reflector are included.

On the other hand, the sidelobes from gaps in the secondary fade out at nearly 8 degrees from the center but are roughly two orders of magnitude stronger than those from the primary gaps, with amplitudes reaching 0 dBi. These sidelobes are also ray-like, but sharper and more evenly distributed than the primary gaps ones. This ray-like shape of the sidelobes mixes degree and sub-degree angular scales, meaning that the sidelobes can introduce systematic effects over a large range of angular scales.

We note that this simulation considered uniform gap widths, which is not the real case. The width of the gaps have an effect on the strength of the features but not on their shape, so non-uniform gap widths are expected to impact only the intensity distribution of the features.

Component	Ω (nstr)
Main beam (Ω_{MB})	428
Sidelobes (Ω_{SL})	19
Spillover	4.4%

Table 1. Main beam (MB) and sidelobe (SL) solid angles from the reflector gaps, and corresponding percentage of spill-over.

2.2 Sidelobe solid angles

The power contribution of the sidelobes is proportional to their solid angle in comparison to the main beam solid angle. We define the main beam solid angle Ω_{MB} as the integral under the normalized beam up to 0.25 degrees from the center and the sidelobes beam Ω_{SL} as the integral beyond 0.25 degrees from the center. A comparison of these solid angles is shown in Table 1, indicating that the sidelobes from open gaps would contribute 4.4% of the power seen by the telescope. This power is distributed over wide angles according to the beam shape described above. Given that the beam is not circularly symmetric, it is necessary to consider the angles at which the beam was projected on the sky during a real observation to fully understand the effects of this beam on the CMB power spectrum measured measured by ACTpol. We explore this in the next section.

3. SIDELOBE EFFECTS ON CMB MAPS

When pointed at the sky, the power received by a detector corresponds to the weighted sum of the sky over the beam, thus a direct projection onto a map produces a representation of the sky convolved by the beam shape. This does not represent a problem for circularly symmetric, unpolarized beams, as the effect can be easily canceled by dividing map power spectrum by the beam window function.[8] However, extended, highly non-symmetric or polarized beams are harder to handle, though they can be incorporated during map-making.[9–11] A simple mapper will average down different orientations of the beam depending on the scan strategy, producing an effective beam which might not be uniform across the map. For the same reason, an asymmetric beam would also produce temperature to polarization leakage, as the scan strategy can favor one polarization over the other.[12] To mitigate this effect, the ACT detector array is designed using pairs of detectors with opposite polarization coupled to the same feedhorn, thus sharing the same beam on the sky and canceling out temperature to polarization leakage. Unfortunately, non-working detectors tend to break detector pairs, leaving single detectors susceptible to produce leakage.

To better understand these effects, we developed a simulation which deprojects a CMB map back into TOD using the asymmetric beam and the actual pointing and detector selection information from real ACT observations. The TOD are then reprojected back to maps, which thus contain the sidelobe contribution.

The power measured by a detector sample can be written as

$$d(\theta_0, \phi_0, \alpha) = \int P(\theta, \phi) B\left(R\{\theta, \phi; \theta_0, \phi_0, q\}\right) \, \mathrm{d}\Omega, \tag{1}$$

where $P(\theta, \phi)$ is the sky power distribution (or Stokes parameter), $B(\rho, \chi)$ is the beam function defined at the origin, and the operator R maps the beam on the sky for a given pointing vector (θ_0, ϕ_0) and parallactic angle of the telescope q, such that

$$\rho = \cos^{-1}\left(\sin(\theta)\sin(\theta_0) + \cos(\theta)\cos(\theta_0)\cos(\phi - \phi_0) \right), \tag{2}$$

$$\chi = \tan^{-1}\left(\frac{\sin(\phi - \phi_0)\cos(\theta_0)}{\cos(\theta)\sin(\theta_0) - \sin(\theta)\cos(\theta_0)\cos(\phi - \phi_0)} \right) - q. \tag{3}$$

If the detector is sensitive to one linear polarization, the sky power P is replaced by the I, Q and U Stokes parameters in Equation 1, producing components d_I, d_Q and d_U respectively, such that the power measured by the detector is

$$d_p = d_I + d_Q \cos 2\psi + d_U \sin 2\psi, \tag{4}$$

where ψ is the polarization angle of the detector on the sky.

To simulate an observation, we need to compute the value of each sample considering all pointings from all detectors. This will produce a synthetic TOD, which can then be projected onto a map for a given pixelization.

3.1 Computational considerations

The size of the computational problem scales quadratically with the angular resolution and linearly with the number of TOD samples considered. To properly model the effect of sidelobes at 8 degrees from the center for a regular ACT map, with 30" pixels, the beam map should have 10^7 pixels. This means that deprojecting a single sample would require a hundred times this number of FLOPs. For example, the ACT field Deep5, which is a 70 deg^2 area centered on Right Ascension 355 degrees and Declination 0 degrees, contains 10^{12} samples. This translates to a total of 10^{21} FLOPs, which is intractable with current computers. This forces us to simplify the problem by reducing the resolution of the beam map and reducing the number of TOD samples considered. It also puts a strong emphasis on the selection of the computer architecture and efficiency of the algorithm.

Given that the operations to compute the beam deprojection are independent, the implementation heavily benefits from massive parallel architectures like GPUs. Modern graphics cards offer several TFLOPS of raw computing power at a moderate cost,[13] being the selected architecture for this project. The software was written in C using the CUDA API[†], optimizing the algorithm to exploit parallelization. Our implementation takes 480 μs to deproject one TOD sample using a 10^6 pixel beam on a single NVIDIA GTX580 card. This is 20 times faster than an equivalent CPU implementation using Intel i7 2600K.

The deprojection of the beam requires aligning the pixels of the input sky map with pixels of the beam map. The proper way to do this is interpolating one of the maps, but this process computationally expensive. Instead, we oversampled the beam map in order to reduce the jitter produced by the misalignment of the pixels. We found that an oversample of four times is enough to control the effect, being still less expensive than interpolating.

3.2 Validation tests

To test our code, we ran a simulation using a Gaussian beam with 0.5 degree FWHM, on a map with resolution of 7'. We compared the result with the same input map convolved with the same Gaussian beam in harmonic space, which is expected to produce the same result.

The results are shown in Figure 3. To the eye the deprojected maps are very similar to the convolved maps. The difference map shows that high-frequency jitter noise is present in the deprojected map. The jitter noise is driven by the central part of the beam and is related to the pixel size with respect to the beam width. This is not a problem for the sidelobe maps that we make, as they do not have such sharp, small scale features. Moreover, since the noise is stronger at angular scales much smaller than the ones of interest, it can be filtered out.

3.3 Sidelobe maps

We ran our simulation on a real ACT observing field. The pointing data comes from observations of the ACT field Deep5. This is large enough to show effects at degree scales, while keeping the computing time low enough.

We used $\approx 7\%$ of the ACT data scans on the field, and half of the available detectors while keeping a uniform sampling over the area, with equivalent number of rising versus setting scans[14] and a uniform distribution of detector angles. We reduced the TOD samples by downsampling the time-streams by a factor of 40. This left us with 4.3×10^8 detector samples to deproject.

Using fewer samples may degrade the amount of averaging seen by the asymmetric beam on the map, reducing the effective symmetrization of the beam and producing non-trivial effects in the map power spectrum. The detector selection was done keeping about half of the detectors forming detector pairs, which is an upper limit to the expected number of broken pairs in a normal observation. For the above reasons, we consider our results an upper limit to the temperature to polarization leakage.

Given that the smallest features of the sidelobes are several arc-minutes across, we limited the resolution on the beam to 7', requiring a beam map with 2.5×10^5 pixels. As we are interested only in the effect of the sidelobes,

[†]www.nvidia.comcuda

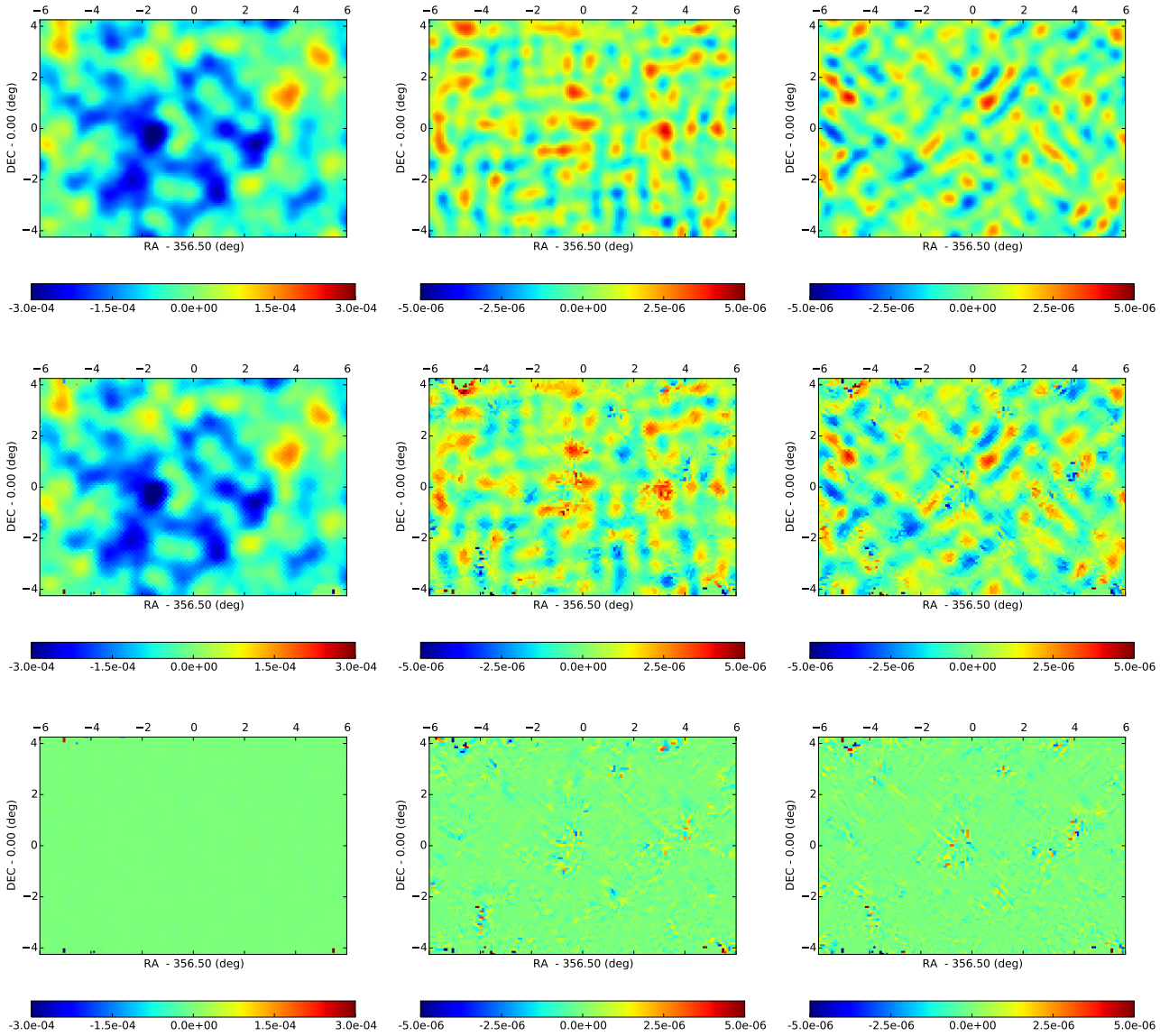

Figure 3. Upper row: CMB map realization smoothed with a 0.5 degree FWHM Gaussian beam in harmonic space. Middle row: beam reprojection simulation output using a pixelized 0.5 degree FWHM Gaussian beam. Both the input and output maps have consistent scales and show very similar structure at degrees angular scale. Bad pixels at the edge as well as jitter in the polarization maps are caused by incomplete sky coverage and TOD downsampling. Bottom row: Difference maps showing better than 0.1% agreement. The discrepancies are driven by pixelization jitter, which is stronger in shallower areas of the scan like edges. All maps are in Kelvin.

we masked the central beam up to 0.25 degrees from the center. This also helps eliminating pixelization jitter noise originated from using pixels larger than the beam FWHM. We ran the simulation on a HEALPIX map with 7' pixels (HEALPIX NSIDE=512), taking less than 15 hours to finish on a single NVIDIA GTX580 card.

Figure 4 shows the input and output maps of these simulations. It is clear that the sidelobes cause measurable pickup as well as leakage, as shown in the second row of plots in the figure. To isolate the contribution of temperature in the resulting Q and U maps, we ran our simulation again with a temperature only map, such that

the power obtained in the Q and U maps corresponds exclusively to leakage from temperature (I) to polarization (Q and U). The results are shown in the third row of the figure. It can be noticed that the leakage is highly non-Gaussian, following the direction of the scan, being stronger in areas with less cross-linking. Finally, to double check our results, we ran again using only paired detectors and a temperature only input map, producing no leakage as expected. These results are shown on the lower row of the figure. We conclude that the effect of the far sidelobes produced by bare panel gaps is significant and must be considered and minimized in the experiment.

We must note that pixels with low number of data samples, or measured with uneven polarization angles, suffer from ill-conditioned pointing matrices, thus getting unstable values. This is the case for around 3% of the pixels. These pixels are excluded from the statistical analysis and zeroed in the plots for better visualization.

Map	I_{RMS} [nK]	Q_{RMS} [nK]	U_{RMS} [nK]
CMB Input	111930	3920	3910
Sidelobes (half pairs)	4180 (3.73%)	47 (0.12%)	45 (0.11%)
Sidelobes (I only, half pairs)	3931 (3.51%)	22 (0.05%)	23 (0.06%)
Sidelobes (I only, only pairs)	4012 (3.58%)	0.0 (0.00%)	0.0 (0.00%)

Table 2. RMS power in CMB input maps and sidelobe maps. The last row shows the results for a sidelobe map obtained after zeroing the Q and U components of the input maps. Each simulation was run using 352 single detectors.

Table 2 shows the RMS power measured in all the maps from Figure 4. The residual temperature fluctuations in the sidelobe map are consistent with the 4% contribution indicated by the beam solid angle estimates in Table 1. We also see that the residual power in the Q and U sidelobe maps is around 0.1% of the Q and U inputs. This is consistent with the fact that the sidelobe beam filters out small angular scales, where most of the polarized power is present, while the temperature maps contains proportionally more large-scale power. Around half of that power is still present after zeroing the Q and U components of the input map, implying that the dominant effect is temperature to polarization leakage. Comparing the RMS of the Q and U maps produced by I only to the input temperature signal, we conclude that the sidelobes leak 0.02% of the temperature power into polarization.

4. CONCLUSIONS

In this work, we successfully modeled the effects that open, uniform gaps between panels in the reflectors would produce on the telescope beam. This simulation considers the upper limit case in which the gaps are not covered with aluminum tape, but a slight underestimate in that only PO is used to model diffraction. We found that the sidelobes are ray-like, extending from the center in all directions with vertical symmetry. They account for around 4.4% of the total beam solid angle, contributing with a significant fraction of the measured power. The shape of the sidelobes contain structure with angular scales ranging from several arcminutes to several degrees, so we expect them to manifest in the map power spectrum at multipoles below $\ell = 225$.

To fully understand the effect of these sidelobes on the observed maps, we developed a code to realistically simulate a CMB observation done with a circularly asymmetric, unpolarized beam projected on the sky at angles defined by a real scan strategy. We ran this simulation using pointing information from the ACT field Deep5 and found an upper limit to the temperature to polarization leakage produced by sidelobes on the order of 0.02% of the temperature power. The leakage in ACT from an unpolarized beam is strongly dependent on the number of single detectors (broken pairs), so it can be controlled by minimizing the number of single detectors used in the analysis. The sidelobe calculations could not be completed for a polarized beam, a case that was not studied in this work.

Our results demonstrate the importance of fully characterizing the sidelobes produced by the reflector gaps and their systematic effects on the maps, together with the need to implement methods to incorporate them into the scientific data analysis. We emphasize that we have simulated worst case scenario, with open gaps of uniform size, no tape on them and incomplete TOD data sampling with causes incomplete symmetrization of the beam.

The temperature to polarization leakage is most significant at low TOD frequencies, where the atmosphere signal is stronger. This effect is mitigated by modulating the incoming polarized signal to higher TOD frequencies, effectively filtering out the atmosphere. For this and other reasons, ACT is currently implementing Half Wave Plates (HWP) in front of the receiver, which will reduce the leakage from sidelobes even more.

4.1 Future work

To improve the results presented here, we plan on incorporating more realistic properties of the gaps. This includes representing the actual population of gap widths, and simulating the effects of covering the gaps with aluminum tape of a certain width and thickness within the context of geometric theory of diffraction. The simulations will also be extended to wider angles to see the full extension of the far sidelobes.

With respect to the map simulations, we plan to extend them to a wider area to obtain a better representation of large scale features picked up by the sidelobes. This will require a more efficient code running current generation GPUs, and more computational time. We will repeat these simulations using many realizations of the CMB map, producing enough simulated data to perform a proper spectral analysis of the effect. Finally, we plan to compare these results to ACT sun and moon maps of the sidelobes, generating a model that will allow us to mitigate the systematic effect of reflector gap sidelobes in the ACT maps at the map making stage.

ACKNOWLEDGMENTS

PF is financed by a VRI grant from PUC. R.D. thanks CONICYT for grants FONDECYT 1141113, PIA Anillo ACT-1417 and BASAL PFB06. LM is funded by the ALMA-CONICYT Astronomy Program (project 31140004).

REFERENCES

[1] Fowler, J. W., Niemack, M. D., Dicker, S. R., Aboobaker, A. M., Ade, P. A. R., Battistelli, E. S., Devlin, M. J., Fisher, R. P., Halpern, M., Hargrave, P. C., Hincks, A. D., Kaul, M., Klein, J., Lau, J. M., Limon, M., Marriage, T. A., Mauskopf, P. D., Page, L., Staggs, S. T., Swetz, D. S., Switzer, E. R., Thornton, R. J., and Tucker, C. E., "Optical design of the Atacama Cosmology Telescope and the Millimeter Bolometric Array Camera," *ao* **46**, 3444–3454 (June 2007).

[2] Hincks, A. D., Acquaviva, V., Ade, P. A. R., Aguirre, P., Amiri, M., Appel, J. W., Barrientos, L. F., Battistelli, E. S., Bond, J. R., Brown, B., Burger, B., Chervenak, J., Das, S., Devlin, M. J., Dicker, S. R., Doriese, W. B., Dunkley, J., Dünner, R., Essinger-Hileman, T., Fisher, R. P., Fowler, J. W., Hajian, A., Halpern, M., Hasselfield, M., Hernández-Monteagudo, C., Hilton, G. C., Hilton, M., Hlozek, R., Huffenberger, K. M., Hughes, D. H., Hughes, J. P., Infante, L., Irwin, K. D., Jimenez, R., Juin, J. B., Kaul, M., Klein, J., Kosowsky, A., Lau, J. M., Limon, M., Lin, Y.-T., Lupton, R. H., Marriage, T. A., Marsden, D., Martocci, K., Mauskopf, P., Menanteau, F., Moodley, K., Moseley, H., Netterfield, C. B., Niemack, M. D., Nolta, M. R., Page, L. A., Parker, L., Partridge, B., Quintana, H., Reid, B., Sehgal, N., Sievers, J., Spergel, D. N., Staggs, S. T., Stryzak, O., Swetz, D. S., Switzer, E. R., Thornton, R., Trac, H., Tucker, C., Verde, L., Warne, R., Wilson, G., Wollack, E., and Zhao, Y., "The Atacama Cosmology Telescope (ACT): Beam Profiles and First SZ Cluster Maps," *apjs* **191**, 423–438 (Dec. 2010).

[3] Dünner, R., Gallardo, P., Wollack, E., Henriquez, F., and Jerez-Hanckes, C., "Far sidelobes measurement of the atacama cosmology telescope," (2012).

[4] Thornton, R. J., Ade, P. A. R., Aiola, S., Angile, F. E., Amiri, M., Beall, J. A., Becker, D. T., Cho, H., Choi, S. K., Corlies, P., Coughlin, K. P., Datta, R., Devlin, M. J., Dicker, S. R., Dunner, R., Fowler, J. W., Fox, A. E., Gallardo, P. A., Gao, J., Grace, E., Halpern, M., Hasselfield, M., Henderson, S. W., Hilton, G. C., Hincks, A. D., Ho, S. P., Hubmayr, J., Irwin, K. D., Klein, J., Koopman, B., Li, D., Louis, T., Lungu, M., Maurin, L., McMahon, J., Munson, C. D., Naess, S., Nati, F., Newburgh, L., Nibarger, J., Niemack, M. D., Niraula, P., Nolta, M. R., Page, L. A., Pappas, C. G., Schillaci, A., Schmitt, B. L., Sehgal, N., Sievers, J. L., Simon, S. M., Staggs, S. T., Tucker, C., Uehara, M., van Lanen, J., Ward, J. T., and Wollack, E. J., "The Atacama Cosmology Telescope: The polarization-sensitive ACTPol instrument," *ArXiv e-prints* (May 2016).

[5] Henderson, S. W., Allison, R., Austermann, J., Baildon, T., Battaglia, N., Beall, J. A., Becker, D., De Bernardis, F., Bond, J. R., Calabrese, E., Choi, S. K., Coughlin, K. P., Crowley, K. T., Datta, R., Devlin, M. J., Duff, S. M., Dunkley, J., Dünner, R., van Engelen, A., Gallardo, P. A., Grace, E., Hasselfield, M., Hills, F., Hilton, G. C., Hincks, A. D., Hložek, R., Ho, S. P., Hubmayr, J., Huffenberger, K., Hughes, J. P., Irwin, K. D., Koopman, B. J., Kosowsky, A. B., Li, D., McMahon, J., Munson, C., Nati, F., Newburgh, L., Niemack, M. D., Niraula, P., Page, L. A., Pappas, C. G., Salatino, M., Schillaci, A., Schmitt, B. L., Sehgal, N., Sherwin, B. D., Sievers, J. L., Simon, S. M., Spergel, D. N., Staggs, S. T., Stevens, J. R., Thornton, R., Van Lanen, J., Vavagiakis, E. M., Ward, J. T., and Wollack, E. J., "Advanced ACTPol Cryogenic Detector Arrays and Readout," *Journal of Low Temperature Physics* (Mar. 2016).

[6] Shore, R. A. and Yaghjian, A. D., "Application of incremental length diffraction coefficients to calculate the pattern effects of the rim and surface cracks of a reflector antenna," *IEEE transactions on antennas and propagation* **41** (1993).

[7] Górski, K. M., Hivon, E., Banday, A. J., Wandelt, B. D., Hansen, F. K., Reinecke, M., and Bartelmann, M., "HEALPix: A Framework for High-Resolution Discretization and Fast Analysis of Data Distributed on the Sphere," *apj* **622**, 759–771 (Apr. 2005).

[8] Page, L., Barnes, C., Hinshaw, G., Spergel, D. N., Weiland, J. L., Wollack, E., Bennett, C. L., Halpern, M., Jarosik, N., Kogut, A., Limon, M., Meyer, S. S., Tucker, G. S., and Wright, E. L., "First-Year Wilkinson Microwave Anisotropy Probe (WMAP) Observations: Beam Profiles and Window Functions," *apjs* **148**, 39–50 (Sept. 2003).

[9] Tristram, M., Macías-Pérez, J. F., Renault, C., and Hamilton, J.-C., "Asymfast: A method for convolving maps with asymmetric main beams," *Phys. Rev. D* **69**, 123008 (Jun 2004).

[10] Wallis, C. G. R., Brown, M. L., Battye, R. A., Pisano, G., and Lamagna, L., "Removing beam asymmetry bias in precision CMB temperature and polarisation experiments," *ArXiv e-prints* (Jan. 2014).

[11] Mitra, S., Sengupta, A. S., Ray, S., Saha, R., and Souradeep, T., "Cosmic microwave background power spectrum estimation with non-circular beam and incomplete sky coverage," *MNRAS* **394**, 1419–1439 (Apr. 2009).

[12] Das, S., Mitra, S., and Paulson, S. T., "Effect of noncircularity of experimental beam on cmb parameter estimation," *Journal of Cosmology and Astroparticle Physics* **2015**(03), 048 (2015).

[13] Che, S., Boyer, M., Meng, J., Tarjan, D., Sheaffer, J. W., and Skadron, K., "A performance study of general-purpose applications on graphics processors using cuda," *J. Parallel Distrib. Comput.* **68**, 1370–1380 (Oct. 2008).

[14] Dünner, R., Hasselfield, M., Marriage, T. A., Sievers, J., Acquaviva, V., Addison, G. E., Ade, P. A. R., Aguirre, P., Amiri, M., Appel, J. W., Barrientos, L. F., Battistelli, E. S., Bond, J. R., Brown, B., Burger, B., Calabrese, E., Chervenak, J., Das, S., Devlin, M. J., Dicker, S. R., Bertrand Doriese, W., Dunkley, J., Essinger-Hileman, T., Fisher, R. P., Gralla, M. B., Fowler, J. W., Hajian, A., Halpern, M., Hernández-Monteagudo, C., Hilton, G. C., Hilton, M., Hincks, A. D., Hlozek, R., Huffenberger, K. M., Hughes, D. H., Hughes, J. P., Infante, L., Irwin, K. D., Baptiste Juin, J., Kaul, M., Klein, J., Kosowsky, A., Lau, J. M., Limon, M., Lin, Y.-T., Louis, T., Lupton, R. H., Marsden, D., Martocci, K., Mauskopf, P., Menanteau, F., Moodley, K., Moseley, H., Netterfield, C. B., Niemack, M. D., Nolta, M. R., Page, L. A., Parker, L., Partridge, B., Quintana, H., Reid, B., Sehgal, N., Sherwin, B. D., Spergel, D. N., Staggs, S. T., Swetz, D. S., Switzer, E. R., Thornton, R., Trac, H., Tucker, C., Warne, R., Wilson, G., Wollack, E., and Zhao, Y., "The Atacama Cosmology Telescope: Data Characterization and Mapmaking," *apj* **762**, 10 (Jan. 2013).

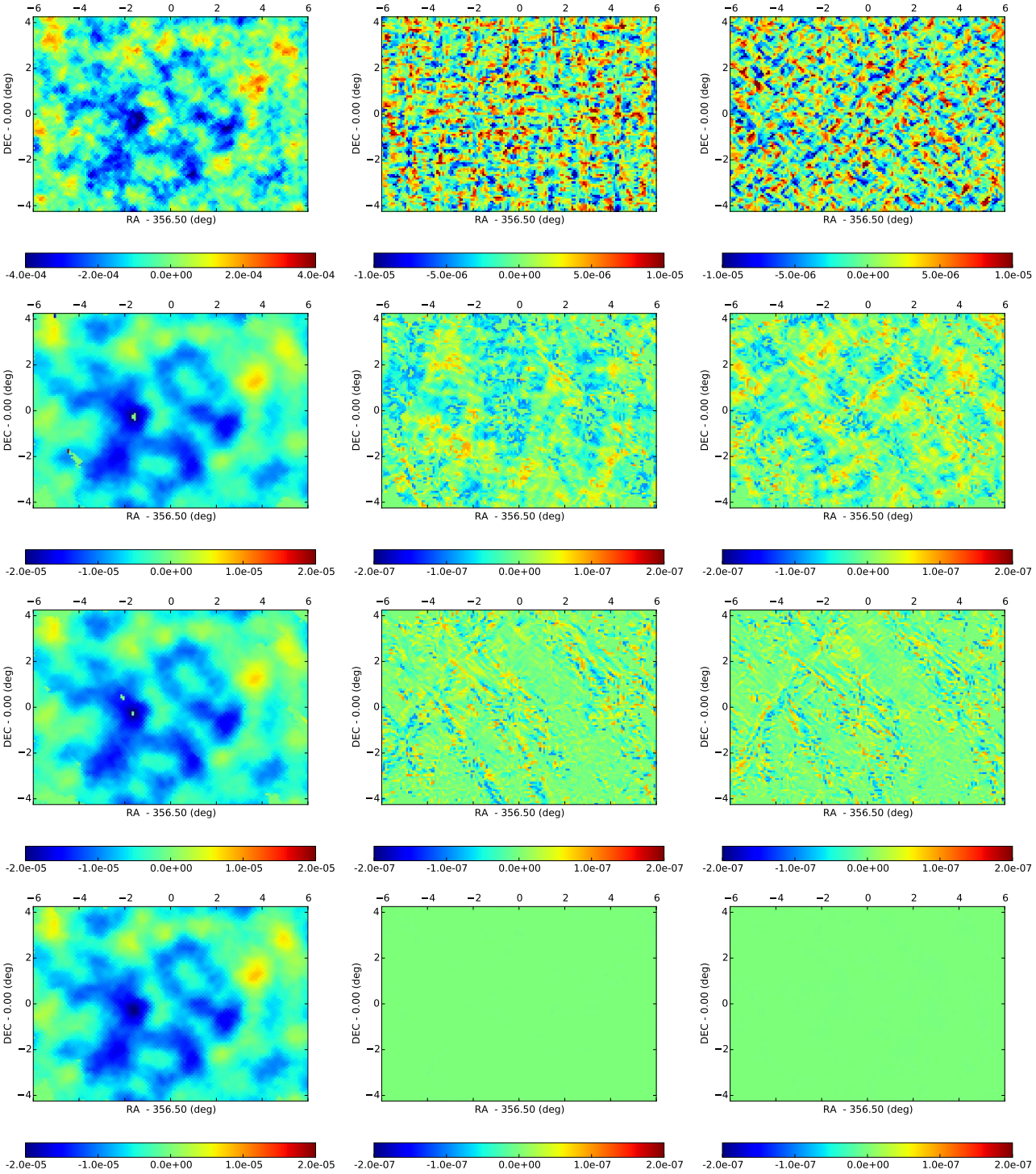

Figure 4. First row: input CMB map realization components (I, Q and U from left to right) used for the simulation. Second row: respective sidelobe reprojection map components obtained by using the sidelobe part of the beam and the scan pointing information of ACT Deep5 field. Third row: same as second row but zeroing the Q and U components of the CMB input map, such that the temperature to polarization leakage effect is isolated. Forth row: same as third row but using only paired detectors in the simulation, canceling out the temperature to polarization leakage. All maps are in Kelvin. Notice that the scale of the sidelobe maps, compared to the input maps, is 20 times lower for I and 50 times for Q and U. Ill-defined pixels in the maps were set to zero for improving the visualization.